
Article:
Koutas, L. orcid.org/0000-0002-7259-6910, Triantafillou, T.C. and Bousias, S.N. (2014) Analytical modeling of masonry-infilled RC frames retrofitted with textile-reinforced mortar. Journal of Composites for Construction, 19 (5). 04014082. ISSN 1090-0268

https://doi.org/10.1061/(ASCE)CC.1943-5614.0000553

Analytical Modeling of Masonry-Infilled RC Frames Retrofitted with Textile-Reinforced Mortar

L. Koutas[1]; T. C. Triantafillou, M.ASCE[2]; and S. N. Bousias, M.ASCE[3]

[1] Graduate student, Dept. of Civil Engrg., Univ. of Patras, Patras GR-26500, Greece. Email: koutasciv@gmail.com
[2] Professor, Dept. of Civil Engrg., Univ. of Patras, Patras GR-26500, Greece. Email: ttriant@upatras.gr
[3] Associate Professor, Dept. of Civil Engrg., Univ. of Patras, Patras GR-26500, Greece. Email: sbousias@upatras.gr

Abstract:

The present paper proposes an analytical approach for modeling the behavior of textile-reinforced mortar (TRM)-strengthened masonry-infilled reinforced concrete (RC) frames under seismic loading. The model falls into the discrete diagonal-element type and is based on the use of single-strut and single-tie elements to represent the infill panel. It builds on the results of past experimental studies by the authors in which the application of TRM jacketing was proved to be effective for the seismic retrofitting of masonry infilled RC frames. The model is implemented in the non-linear finite element code *Opensees*, with the parameters of the diagonal elements being determined from a series of tests on TRM coupons and masonry specimens. Finally, the results of the numerical analyses are compared with the experimental data of cyclic tests on three-story masonry infilled RC frames, as-build and after retrofitting. It is shown that the model developed herein adequately accounts for the TRM-strengthening contribution to the global response of masonry infilled frames.

Keywords: masonry infill; modeling; OpenSees; reinforced concrete; seismic retrofitting; strengthening; textile-reinforced mortar (TRM).

Introduction and Background

The use of textile-reinforced mortar (TRM) as strengthening material for substandard reinforced concrete (RC) members (Triantafillou and Papanicolaou 2006, Triantafillou et al. 2006, Bournas et al. 2007, Bournas et al. 2009, Al-Salloum et al. 2011) and for masonry panels (Papanicolaou et al. 2007, Papanicolaou et al. 2008, Harajli et al. 2010, Parisi et al. 2013, Babaeidarabad et al. 2014) has been experimentally investigated in the past and has been reported to be effective in the majority of the cases. In the recent past the authors presented a concept for strengthening masonry-infilled RC frames with TRM. Following the investigation of different infill-frame connection methods on small scale masonry sub-assemblies (Koutas et al. 2014a), this new strengthening technique was applied for the first time in a large scale three-story masonry-infilled RC frame (Koutas et al. 2014b). The experimental results clearly indicated that the TRM layers externally bonded to the infill surfaces and anchored to the surrounding frame members, contributed significantly to the global lateral response of the infilled frame. Nevertheless, for the method to be widely employed, support from properly calibrated and validated analytical tools is needed. The development of an analytical model that captures the salient features of the response of TRM-retrofitted infilled frames, as accurately as possible, is the main focus of the work presented in this study.

Modeling the in-plane behavior of masonry infills has been the field of study for many researchers over the past 50 years, resulting in a significant number of different approaches. The level of modeling sophistication varies from the simpler approaches that make use of a single-strut element along the compressed diagonal of the infill panel, to the more complicated ones that make use of highly discretized 2D finite elements along with interface elements in order to accurately account for the “micro-scale” behavior of the infill panel. Notwithstanding the inherent limitations of the single-strut model, such as the inability to

account for local effects (additional shear forces and bending moments in the surrounding frame members), it has been adopted in many evaluation studies (e.g. Madan et al. 1997, Kappos et al. 1998, Dolsek and Fajfar 2002, Skafida et al. 2014) yielding satisfactory agreement between analytical and experimental results. According to Chrysostomou and Asteris (2012), the general consensus is that a single equivalent-strut approach (two struts per panel for reversed cyclic loading analysis, one across each diagonal) may be successfully used for design and evaluation studies of infilled frame systems. It is noted that the above conclusion and the (past) experimental/(present) analytical work performed by the authors, are valid for infills without openings.

On the way to modeling the in-plane behavior of masonry-infilled RC frames retrofitted with composite materials other than TRM, Binici and Ozcebe (2006) introduced the concept of combining a pair of diagonal elements (single-strut and single-tie) connecting the two diagonals of an RC frame portal so as to represent a fiber-reinforced polymer (FRP) retrofitted infill panel (a "macro-modeling" scheme). The concept of modeling FRP-strengthened masonry panels with struts and ties was first introduced by Krevaikas and Triantafillou (2005). In their study, Binici and Ozcebe (2006) assigned simple multi-linear stress strain laws to both elements without defining the hysteretic behavior and they performed pushover analyses. The results of the analyses were compared with the envelope curves of several available experimental results yielding good agreement. In that study the key parameter of the FRP-tie model was the FRP strain, the value of which varied depending on the failure mode. Erol et al. (2012) used the same concept by assigning a linear elastic behavior to the tie element. Yet, they calibrated the strut model in order to fit the experimental results with the results of pushover analyses for three half-scale single-bay, single-story FRP- retrofitted masonry-infilled frames. In the study of Akin et al. (2014) an extensive numerical study on FRP-strengthened masonry-infilled RC frames was conducted

using again the same modeling concept, where the stress-strain law for the FRP-ties was the one initially presented by Binici and Ozcebe (2006). The results of pushover analyses were compared with experimental results of three single-bay, two-story (1/3 scaled) FRP-retrofitted infilled frames, yielding good agreement. Their study also included parametric analyses to investigate the effect of different infill aspect ratios on the performance of the strengthening technique. Finally, in the study of Koutromanos and Shing (2014) a Finite Element modeling scheme (belonging to the group of "micro-models") previously presented by Koutromanos et al. (2011) was utilized to model the seismic behavior of a two-bay, three-story masonry-infilled RC frame with one of its ground floor infills being retrofitted with engineering cementitious composites (ECC) overlays. Results of this study indicated that the use of the proposed analytical method was capable of reproducing the cyclic (hysteretic) behavior of the specimen at both global and local level.

In the present study, an analytical model for describing the behavior of TRM-strengthened masonry-infilled reinforced concrete frames is introduced, which is based on the use of a pair of elements per infill diagonal. The presented analytical approach falls into the category of "macro-modeling" (Asteris et al. 2011), an approach which - due to its simplicity over the more accurate, but much more sophisticated "micro-models" – is widely employed by engineers. The model presented was implemented in the *OpenSees* (McKenna et al. 2000) open-source software and was employed to simulate the response of a three-story masonry infilled RC frame strengthened with TRM and tested by the authors under cyclic loading. The values of the physical parameters characterizing the response of the infills were derived from standard tests on masonry sub-assemblies, whereas the properties of the composite material used for strengthening were obtained through tensile tests on TRM coupons. Numerical analyses were carried out to validate the model adopted for the diagonal strut/tie elements. Model predictions are shown to compare satisfactorily with the experimentally observed

response results (Koutas et al. 2014b) in terms of lateral force-displacement response and other response characteristics, such as stiffness and energy dissipation.

Analytical modeling

Modeling Scheme

When flexibility, numerical robustness and ease in practical application need to be collectively satisfied, the introduction of diagonally placed strut/tie elements simulating the behavior of infilling in RC frames has been the method of choice (Fig. 1). Furthermore, when modeling of retrofitted masonry infills - via conventional approaches, or employing advanced materials - is of concern, the additional parameters entering the picture induce further complications, making the above three requirements even more called for. The simplified approach of diagonal struts/ties representing the response of retrofitted masonry infilled RC frames is here exploited further for the case of TRM-retrofitted infills. A pair of alternatively activated elements (a compression-only strut and a tension-only tie) is placed along each diagonal of each portal, as a macroscopic simulation of the experimental response. During a time increment of the dynamic response of the structure the strut element mimics the behavior of the diagonal that is under a compressive stress state, whereas the tie – which is usually employed only in retrofitted infilled frames - accounts for the behavior along the opposite (tensioned) diagonal, relying on the externally bonded material to carry the developing tensile forces.

Strut-element model

For the strut element the model of Fardis and Panagiotakos (1997) has been adopted. Under the simplifying assumption that the lateral displacement, δ, equals the inter-story drift, the model of an infill panel under lateral deformation is represented by the shear force, V, versus

lateral displacement, δ, multi-linear backbone curve of Fig. 2a. This curve, which in the absence of openings is symmetric for the two directions of loading, is characterized by the following four stages:

- Stage I: The masonry responds in an uncracked state until reaching the cracking shear force V_{cr} (point 'A') at a displacement $\delta_{cr}=V_{cr}/K$, where K denotes the panel elastic lateral stiffness.
- Stage II: The body of the infill cracks, but the capacity of the infill has not yet being reached. The current slope of the ascending branch is a fraction p of the initial elastic stiffness K. Stage II ends when the lateral force capacity of the infill panel, V_u, is reached at a displacement δ_u (point 'U'). The secant stiffness at point 'U' is denoted as K_u.
- Stage III: The descending branch during Stage III reflects the gradual reduction in resistance up to the point 'R', where the residual strength of the infill, V_{res}, is reached at a displacement δ_{res}. The negative tangent stiffness equals a fraction p_1 of the initial elastic stiffness K.
- Stage IV: The infill sustains the same residual shear force, V_{res}, under increasing lateral displacements. It is noted that this stage is not usually of practical interest as other effects associated to the global response of the framed structure occur under large displacements (i.e. triggering of a collapse mechanism due to failure in the RC frame members, or due to P-Δ effects).

For cyclic loading, the hysteretic model proposed by Fardis and Panagiotakos (1997) relies upon simple linear hysteresis rules capable of representing the basic mechanics of the in-plane behavior of an infill panel (Fig. 2b). In particular, the model accounts both for stiffness and strength degradation under cyclic loading, while at the same time it can reproduce the "pinching" effect related to the contribution of shear in response. A great advantage of this model over other hysteretic models is that the shape of the hysteresis loops is controlled by

only three parameters, namely α, β and γ, with their value in the range from 0 to 1. Parameter α is associated to the strength degradation; a value equal to 1 signals the absence of any strength degradation. Parameter β controls the level of the resistance (βV_u or $\beta V_u'$) at which the slope (equal to the elastic stiffness, K) of the branch unloading from the envelope curve changes to that of a second (softened) unloading branch; a value equal to 0 corresponds to sliding in shear without any resistance. Finally, by controlling the parameter γ the "pinching" effect can be reproduced. In particular, γ determines the displacement at which the initial softer reloading branch changes to the second stiffer reloading branch at a level of resistance equal to βV_u (or $\beta V_u'$); as γ increases, the "pinching" effect becomes more pronounced. A more detailed description of the hysteretic model can be found in Fardis (2009).

To fully describe the cyclic behavior of an infill panel with the geometry shown in Fig. 3, the following model parameters are needed for the diagonal strut element:

- The initial cracking strength, V_{cr}, which can be calculated as $V_{cr} = \tau_{cr} A$, where τ_{cr} is the diagonal cracking stress (determined from diagonal compression tests on wallettes) and $A=L_{cl}\ t_w$ is the shear stress area, with L_{cl} and t_w denoting the infill clear length and thickness, respectively.
- The initial stiffness, determined as $K=GA/H_{cl}$, where H_{cl} is the clear height of masonry and G is the shear modulus, also determined from wallette diagonal compression tests.
- The ultimate strength V_u, which depends on the failure mechanism, can be obtained from several equations available in the literature (e.g. Stafford Smith and Carter 1969, Mainstone 1971, Paulay and Priestley 1992, Saneinejad and Hobbs 1995). In this study, Eq. (1) presented by Mainstone (1971) for the failure of brick infills under compression (corner crushing) was found to yield the best agreement between experimental and analytical results, when employed for the strut model of the control (unretrofitted) specimen (see "Numerical Simulations" Section).

$$V_u = 0.56(\lambda H)^{-0.875} f_w H t_w \cot\theta_{str} \quad (1)$$

where:

$$\lambda = \left(\frac{E_w t_w \sin 2\theta_{str}}{4 E_c I_c H_{cl}} \right)^{\frac{1}{4}} \quad (2)$$

In the above, f_w is the masonry compressive strength, θ_{str} =arctan(H_{cl} /L_{cl}) is the inclination of the diagonal strut to the horizontal, E_c and E_w are the elastic moduli of the concrete frame members and of the masonry infill, respectively, H is the idealized story height (Fig. 3), and I_c is the moment of inertia of the column section with respect to the axis perpendicular to the plane of the infill panel.

- The secant stiffness to ultimate resistance, K_u, which according to Fardis (2009) can be obtained from Eq. (3) based on the properties of the elastic diagonal strut with a thickness t_w and a width w_{inf}. The value of t_w to be used in the calculations is the actual thickness of the wall, whereas w_{inf} can be calculated from Eq. (4), as proposed by Mainstone (1971).

$$K_u = E_w (w_{\inf} t_w) \cos^3 \theta_{str} / L_{cl} \quad (3)$$

$$w_{\inf} = \frac{0.175 L_{cl}}{\cos\theta_{str} (\lambda \mathrm{H})^{0.4}} \quad (4)$$

- The post-ultimate softening ratio p_1.
- The residual force, V_{res}.
- The three parameters controlling the shape of the hysteresis loops, α, β and γ.

The values of parameters p_1, V_{res}, α, β and γ as proposed by Fardis (2009) after calibration with limited test results (Stylianidis 1985, Zarnic and Tomazevic 1985), are 0.05, 0.5V_u, 0.15, 0.1 and 0.8, respectively. In the present study the values of these parameters were calibrated on the basis of the unretrofitted specimen results and were used for modeling the strut in the retrofitted specimen. It was found that values of 0.015, 0.5V_u, 0.15, 0.2 and 0.3 for p_1, V_{res}, α,

β and γ, respectively, provide good agreement between the analytical and experimental results for the unretrofitted specimen (see "Numerical Simulations" Section).

All the above refer to the horizontal shear force in the infill panel, V, and the horizontal displacement between the top and the bottom of the infill, δ (Fig. 2a). Hence, before assigning the values defining the monotonic curve to to the strut element, a necessary step must precede. This intermediate step is the geometric transformation of the forces and the displacements from the horizontal to the diagonal direction. If F is the axial force in the strut and dL_{str} is the axial shortening of the strut, then the pairs V-δ and F-dL_{str} are interchangeable through Eqs (5) and (6).

$$V = F\cos\theta_{str} \tag{5}$$

$$dL_{str} = \left(\frac{L_{cl}}{H_{cl}}\sin\theta_{str}\right)\delta \tag{6}$$

It is noted that the strut element employed in the numerical analyses was implemented with a tension "cut-off", which practically means that the shaded part in the model shown in Fig. 2b is eliminated.

Tie-element model

To account for the contribution of the externally bonded layers of TRM to the response of the masonry infill under lateral cyclic loading, and, ultimately, to the global response of the infilled frame, an equivalent-tie element model was developed for the panel diagonal under tension. Based on the macroscopic behavior of the TRM layers in the tests perfomed by the authors (Koutas et al. 2014b), the tie axial (tensile) force, F_t, versus tie axial elongation, dL_{tie}, response is modeled as a bi-linear curve (Fig. 4). Should the TRM behave as linear elastic up to the rupture of the textile fibers (point 'U' in Fig. 4), the model would comprise a single linear elastic branch up to a force level corresponding to the ultimate tensile force of the tie,

F_{tu}. However, experimental observations have revealed that, even at very large lateral displacements, the fibers of the textile did not rupture. Under large lateral displacements induced on the panel the textile sustains large shear deformations, while maintaining its structural integrity and depicting a "pseudo-ductile" response. Hence, the response is actually linear elastic up to a lower force level (point 'A'), defined as the effective tensile force, F_{te}. For displacements larger than that corresponding to the effective tensile force (i.e. larger than δ_{te}), the monotonic curve follows a second linear branch with a stiffness softening ratio p_t. The model developed, except for the response under monotonic loading, accounts also for the hysteretic response under cyclic loading. The hysteresis rules of the tie model, presented in Fig. 4, comprise the same linear unloading/reloading rules with the ones in the strut model. Parameters α_t and γ_t control the shape of the hysteresis loops, while parameter β_t controlling the change of slope of the second unloading branch, is taken as nil, reflecting the shear sliding behavior of the retrofitting material from unloading to reloading in the opposite direction, at large deformations.

Consequently, to fully describe the behavior of the tie element, the following parameters need to be determined: (a) the effective axial tensile force, F_{te} , (b) the elastic stiffness, K_t , (c) the post-ulimate softening ratio, p_t , and (d) the set of parameters α_t , γ_t. For calculating the effective axial tensile force, F_{te}, an analytical model was developed in this study. This model builds on the derivation in Triantafillou and Papanicolaou (2006) for the contribution of the textile-reinforced mortar jacket to the shear resistance of shear deficient reinforced concrete members. Assuming an infill panel with length L_{cl} and height H_{cl}, the tie connecting two opposite corners forms an angle $\theta_{tie} = \theta_{str}$ =arctan(H_{cl} /L_{cl}) to the horizontal. The calculation of the tensile force carried by the TRM in the tie-direction is based on the hypothesis that a crack pattern in the other diagonal direction has been formed. Figure 5a depicts a simple, yet representative of test observations, crack pattern that can be assumed;

comprises a single multi-linear crack connecting the bottom with the top corner along the infill's diagonal. For the sake of generality, one of the edges of the crack is shifted vertically at a distance equal to H_{con}, to represent the case that the crack initiates from the point at which the diagonal strut loses contact with the column. This tri-linear crack formation represents in a simple way the dominant diagonal crack pattern observed on the body of the wall in brick-infilled frames with aspect ratio $L_{cl}/H_{cl}>1$; a diagonal (stepped) crack starting from a region close to the top of the, say the left, column, becoming horizontal at wall mid-height, finally re-directing along the diagonal towards the bottom of the right column. Given that the angles of the two inclined branches of the crack to the horizontal, $\theta_{1\alpha}$ and $\theta_{1\beta}$, are approximately equal (due to the step-wise crack formation tracing the brickwork steps), the tri-linear crack is equivalent to the bi-linear one shown in Fig. 5b in terms of the resulting forces in the tie-direction.. This crack comprises two branches: a first-diagonal with a length $L_{cr,1}$ and an inclination θ_1 to the horizontal, and a second-horizontal with a length $L_{cr,2}$. Given this crack pattern, the tensile force carried by the TRM layers is calcutated by summing the contribution of the textile fibers crossing the crack, in each direction i of the textile fiber rovings. This force is expressed in such a way so as to directly refer to the direction of the tie. In the general case, where a textile comprises fiber rovings in two orthogonal directions, with a spacing between fiber rovings in direction i equal to $mesh,i$ and an inclination of roving direction to the horizontal equal to α_i, one can calculate the angle β_i of each roving direction to the level normal to the tie-axis (Fig. 5c) as $\beta_1 = \alpha_1 + \theta_h$ and $\beta_2 = \alpha_2 - \theta_h$, where $\theta_h = 90^o - \theta_{tie}$ is the angle of the projection level to the horizontal. Finally, supported by Fig. 5b, the effective axial force along the direction of the tie can be calculated as:

$$F_{te} = \sum_{i=1}^{2}\sum_{j=1}^{2} \frac{A_{t,i}}{s_i}\left(\varepsilon_{te,i}E_{t,i}\right) d_j \left[\cot\theta_{cr,j} + \left(2i-3\right)\cot\beta_i\right]\sin\beta_i \qquad (7)$$

where:

$$s_i = \frac{mesh,i}{\sin\beta_i} \tag{8}$$

$$d_j = L_{cr,j}\sin\theta_{cr,j} \tag{9}$$

$$L_{cr,1} = \frac{(H_{cl} - H_{con})}{\sin\theta_1} \tag{10a}$$

$$L_{cr,2} = L_{cl} - L_{cr,1}\cos\theta_1 \tag{10b}$$

$$\theta_{cr,1} = 90^o - \theta_{tie} - \theta_1 \tag{11a}$$

$$\theta_{cr,2} = \theta_h \tag{11b}$$

In Eq. (7), $A_{t,i}$ is the cross-section area of the TRM in the direction i, calculated as:

$$A_{t,i} = n_s n_t t_t mesh,i \tag{12}$$

where: n_s is the number of the strengthened sides of the infill panel (n_s=1 or 2); n_t is the number of TRM layers per side; t_t is the thickness of each TRM layer (t_t=4 mm in this study, for consistency with the TRM tests on coupons - see next Section); and *mesh,i* is the spacing between fiber rovings in direction i.

The value of the angle θ_1 can be estimated on the basis that the diagonal crack is a linear approximation of the stepped crack. For a masonry infill constructed from units with dimensions $b_{br}\times d_{br}$ (Fig. 3) and of equal-thickness head and bed mortar joints, angle θ_1 can be derived as:

$$\theta_1 = \tan^{-1}\frac{2b_{br}}{d_{br}} \tag{13}$$

Parameter ε_{ti} in Eq. (7) reflects the "effective" strain of the TRM in direction i (as in Triantafillou and Papanicolaou 2006); it is a crucial parameter for the tie-model. Due to the lack of a sufficiently large databank of test results on masonry infill walls strengthened with TRM, a reliable estimation of the effective strain has not yet been achieved. One of the results of this study is the calibration of the developed tie-model regarding the "effective" strain on the basis of experimental results; a sensitivity analysis on the influence of the value

adopted for the effective strain has also been performed and presented in the "Numerical Simulations" Section.

The initial elastic axial stiffness of the tie can be calculated from Eq. (14), which is based on the format $K=EA/L$:

$$K_t = \sum_{i=1}^{2}\sum_{j=1}^{2} E_{t,i}\left\{\frac{A_{t,i}}{s_i} d_j \left[\cot\theta_{cr,j} + (2i-3)\cot\beta_i\right]\sin\beta_i\right\} / L_{e,tie} \quad (14)$$

where: $L_{e,tie}$ is the effective length of the tie which can be expressed as a fraction of the full tie length, L_{tie}. The reason behind this is that the dispersion of cracking along the tie diagonal is limited and not extending to the full tie length. A sensitivity analysis on this parameter was also performed (presented in "Numerical Simulations" Section).

The rest of the model parameters, namely p_t, α_t and γ_t, have been calibrated on the basis of the test results in Koutas et al. (2014b) as presented in the "Numerical Simulations" Section.

Experimental determination of model parameters

Extensive experimental component testing was carried out for providing the physical parameters required for the model. These parameters include: (a) ultimate stress/strain and elastic secant modulus, obtained from tensile tests on textile-reinforced mortar coupons, (b) compressive strength of masonry, obtained from tests on masonry wallettes and (c) diagonal cracking strength and shear modulus of masonry, from diagonal compression on masonry wallettes.

Textile-reinforced mortar tensile tests

In total, twelve specimens with the geometry shown in Fig. 6a were fabricated and tested, with test parameters being the number of textile layers and the orientation of the fibers. The specimens were categorized into two main groups depending on the number of the textile

layers (one in Group 1 and two in Group 2). Each group comprised six specimens with identical geometry except for the thickness (see Fig. 6a). Main groups were further divided into two sub-groups on the basis of fiber orientation; in half of the coupons (three) the fiber rovings of direction "α_1" of the textile (Fig. 6b) were aligned along the specimen axis (Groups 1A, 2A), whereas in the other half the fiber rovings of direction "α_2" of the textile (Fig. 6b) were aligned with the specimen axis (Groups 1B, 2B).

The textile used as reinforcement as well as the mortar used as matrix of the composite material were the same as the ones used in (Koutas et al. 2014b) for the strengthening of the masonry infills. The properties of the textile are summarized in Table 1. The strength properties of the mortar were obtained through flexural and compressive testing according to EN 1015-11 (1993); the mean flexural and compressive strength (average values from three specimens) at 28 days were found to be 4.2 MPa and 18.4 MPa, respectively.

All specimens were subjected to uniaxial tensile loading (Fig. 7a) imposed at a constant displacement rate of 0.02 mm/sec, via a universal testing machine. Specially designed steel flanges fitting exactly the curved parts of the specimens were employed for applying tension, whereas the elongation of the gauge length was monitored through two electrical gauges adjusted to the boundaries of the gauge length. As expected for textile-reinforced cementitious matrix materials, the response of all specimens comprised three distinct branches. During the first stage the specimen remains uncracked, until the first crack occurs within the gauge length. The following stage, characterized by multiple cracks developing within the gauge length (Fig. 7b), is depicted as a plateau in the stress-strain curve. At the final stage, during which the cracking pattern has developed fully, the increase in resistance is almost exclusively due to the textile itself, until rupture of fibers is observed (within the gauge-length, in most cases).

Each of the four shaded regions in the load versus strain plane depicted in Fig. 8 represents a sub-group of the specimens and encloses all three load-strain curves of the specimens of the corresponding sub-group. The properties required for the analytical model, namely the maximum stress, f_t, the strain at ultimate load, ε_{tu} and the secant elastic modulus, $E_t = f_t / \varepsilon_{tu}$, were derived from the experimental results and are summarized in Table 2. It is seen in Fig. 8 that the secant modulus from zero load to failure does not appreciably differ from that during the third stage of the stress-strain curves. Hence, the behavior of the material under uniaxial tension can be approximately described as linear elastic up to failure. The values of stresses in Table 2 were calculated by dividing the ultimate load by a nominal thickness, as the use of the latter is quite convenient for design purposes. A nominal thickness of 4 mm per textile layer was considered in this study. Therefore, any calculation during the analysis procedure that refers to the properties of the TRM is directly linked to the value of nominal thickness.

Compression tests on masonry wallettes

The compressive strength, f_m, and the elastic modulus, E_m, of the masonry perpendicular to the bed joints was experimentally obtained through compression tests on masonry wallettes with dimensions of 500x500 mm and a thickness of 55 mm (equal to the thickness of the masonry units) according to EN 1052-1 (1999).

In total, six specimens were fabricated and tested. Three of them were tested as-built and the rest were tested after strengthening with two layers of TRM applied on one of the faces, thereby reproducing half of the (not connected) two-wythe infill walls of the three-story infilled frames in the study of Koutas et al. (2014b). Therefore, the results in terms of stress are valid for the three-story infilled frames, due to the symmetric strengthening of the infills. The load was applied at a displacement rate of 0.01 mm/s, while axial strain was

measured in a 200 mm-gauge length in the central region of the wallettes. The wallettes consisted of the same materials as those used in Koutas et al. (2014b) and were constructed by the same craftsmen.

In the test results as reported in Table 3 the values of stress have been derived employing as load-bearing area the actual one for the as-built specimens or the total one after excluding the area of the TRM layers for the strengthened specimens. This is, again, more convenient for the analysis/design procedure.

Diagonal compression tests on masonry wallettes

For determining the diagonal cracking strength, τ_{cr}, as well as the shear modulus of the masonry, G, standard diagonal compression tests (RILEM 1994, ASTM 2010) on 13 masonry wallettes were carried out. The prisms, 800x800 mm in size and 55 mm in thickness, were subjected to diagonal compression, with seven of them tested as-built (specimens denoted as DC_CON) and the rest tested after strengthening with TRM layers. In particular, half of the latter received one layer of TRM (DC_1L) with the remaining half receiving two TRM layers (DC_2L). In all retrofitted wallettes the strengthening was applied on one side, to represent the one of two masonry infill wall wythes of the three-story masonry infilled RC frames in Koutas et al. (2014b).

The strengthening materials used both for the building and the masonry wallettes were identical to those used in Koutas et al. (2014b). In fact, as in the case of the specimens described in the previous sub-Section, the wallettes were built and strengthened with the same materials (and mix design, for the mortars) and in parallel to the construction and strengthening of the infilling of the three-story building (Specimen #2) tested in by Koutas et al. (2014b). In addition, the tests on the masonry wallettes were conducted close to the date of testing of the three-story masonry infilled RC frame.

The specimens were subjected to monotonic loading under a displacement rate of 0.01mm/s, with both their diagonally opposite ends (contact points) capped using a steel shoe filled with gypsum material to avoid local stress concentration (Fig. 9a). As shown in Fig. 9b, two steel tubes parallel to the plane of the specimens were employed to prevent out-of-plane displacement of the top load-bearing steel shoe. The deformation of the wallettes was measured along the diagonals in a gauge length equal to 420 mm. The resulting shear-stress versus shear-strain curves of all specimens are plotted in Fig. 10. All unretrofitted wallettes (DC-CON) reached their ultimate strength soon after a main diagonal stepped crack developed, resulting in sudden load drop and splitting of the wallettes (Fig. 9c). In contrast, all retrofitted wallettes (DC-1L, DC-2L) showed a steady response up to ultimate strength, with the TRM layers controlling cracking. After the ultimate load was attained, the previously formed cracks opened wider, but the presence of TRM layers accommodated the resulting large shear deformation of the masonry prism, while providing residual shear resistance. Table 4 summarizes the results for the three tested specimens groups. The shear modulus, G, was calculated as $G=\tau_{cr}/\gamma_{cr}$, where τ_{cr} is the diagonal cracking strength and γ_{cr} is the corresponding shear strain. The diagonal cracking strength was defined as $\tau_{cr} = \tau_{max}$, for the control (unretrofitted) specimens and as $\tau_{cr}=0.7\tau_{max}$, for the retrofitted ones, consistent with a number of studies, including the recent ones of Dizhur et al. (2013), Parisi et al. (2013) and Babaeidarabad et al. (2014).

Numerical simulations

Simulations details

The numerical simulations were done using the software platform *OpenSees* (McKenna et al. 2000). *OpenSees* is an "open-source" software offering a variety of materials and elements and used mainly for non-linear analysis of structures subjected to cyclic or seismic loading. It

was selected on the basis of its flexibility in creating new materials models with specific constitutive laws (e.g. in F-δ terms). Two new such materials were created and implemented in *OpenSees*: an infill strut material and an infill tie material, in accordance with the strut and tie models presented above.

The three-story masonry-infilled RC frame (Fig. 11a) tested by the authors (Koutas et al. 2014b) was numerically simulated using the model configuration shown in Fig. 11b. Two different models, one to simulate the unretrofitted infilled frame and another one to simulate the retrofitted one, were built, with the elements simulating the RC members being identical.

The RC members were modeled via linear *elastic Beam-Column elements* with two non-linear rotational springs at their ends (*zero-length elements* with M-θ constitutive law) to simulate the formation of plastic hinges. A bilinear envelop curve M-θ coupled with a modified Takeda et al. (1970) hysteresis model (modified to include degradation of the unloading stiffness) for the unloading/reloading cycles were employed (the hysteresis model was reproduced in *OpenSees* using the *Hysteretic Materials*, with appropriate parameter values). The properties of the plastic hinges (moment at yielding, ultimate moment, chord rotation at yield and ultimate chord rotation) were determined following the provisions of EN 1998-3 (2005). The stiffness of the rotational springs at the elastic member ends and that of the elastic member were defined according to Ibarra and Krawinkler (2005). All the above parameters are summarized in Table 5.

The infill panels in the unretrofitted frame were modelled with diagonally placed, compression-only struts, whereas in the case of the retrofitted frame, they were modelled with diagonally placed struts and ties activated only in compression and in tension, respectively. Each diagonal (strut/tie) element (*two-node link element* in *OpenSees*) was connected to supplementary nodes at the ends of the element representing the elastic part of the column (*elastic beam-column element* in *OpenSees*). Rotational springs simulating the

inelastic part of the columns (plastic hinges) connected the supplementary nodes to the control nodes at the intersection of the beam-column axes (Fig. 11b).

The properties required for the strut and tie elements in the numerical analyses, as derived from tests on components, are summarized in Tables 6 and 7, respectively. As seen in Table 6, the properties of the strut element that differ significantly between the unretrofitted and the retrofitted specimen are those related to the mechanical properties of the infill up to first cracking (τ_{cr}, V_{cr}, G and K). These differences reflect the significant effect of the TRM layers on the shear cracking strength and the shear modulus of the masonry panel. The values of τ_{cr} and G were taken from the results of the diagonal compression tests presented in the previous section, whereas the values of V_{cr} and K were calculated according to the methodology presented in the "Strut element model" section. On the other hand, the properties of the strut element which are associated with the strut compression properties (f_w, E_w and V_u) are marginally different. These minor differences reflect the limited effect of the TRM layers on the masonry compressive strength and axial stiffness. The values of f_w and E_w were taken from the results of the compression tests presented in the previous section, whereas the value of V_u was calculated using Eq. (1) Finally note that strut parameters α, β and γ - related to the details of the hysteresis rules - are the same in both models.

The axial load applied to the test specimens was simulated as concentrated vertical load at each story basic node. The lateral loading was applied as incremental lateral displacement at the leeward node of the top floor (Fig. 11b), while maintaining an inverted triangular distribution of the horizontal forces at the three floor levels, as imposed in the tests of Koutas et al. (2014b).

Simulation of the unretrofitted infilled frame

Modeling of the unretrofitted frame served for the validation of the strut model that was presented in "Analytical Modeling" Section, with the available experimental results. It is important to clarify that the basic strut properties, namely F_{cr}, K, F_u and K_u were not calibrated from the test results of the three-story frame, but were derived instead via Eqs (1) - (6), using the experimentally obtained values from the tests presented in the previous Section for parameters τ_{cr}, G, f_w and E_w. In contrast, the values assigned to parameters p_1, α, β, and γ were calibrated to best fit the test results of the three-story frame.

The analytically obtained base shear versus top floor displacement envelope curves for varying values of the post-ultimate stiffness softening ratio, p_1, are compared to the corresponding experimental hysteresis loops in Fig. 12a. For the range of the p_1-values examined, p_1=0.015 was selected as the one that fits better the test results in the positive direction of loading. The lack of symmetry in the force-displacement experimental response of the unretrofitted infilled frame was due to the shear failure of a ground story column; such response cannot be captured by the numerical model adopted. This type of failure is not of interest in this study – in fact, such failure was precluded in the retrofitted infilled frame by a-priori local shear strengthening of the columns. As shown in Figs 12b, c, the shape of the hysteresis loops was better reproduced analytically for α = 0.15, β = 0.2 and γ = 0.3 (the response in the negative loading direction is again ignored), hence these were the values adopted for the strut elements.

A comparison between analytical and experimental results for the unretrofitted specimen is given in Fig. 13a, b and c in terms of global lateral stiffness, cumulative hysteretic energy and first floor displacements, respectively. As illustrated in these figures, the agreement between modeling and test results is quite satisfactory.

Simulation of the retrofitted infilled frame

Following the validation of the strut model on the basis of the test results of the unretrofitted infilled frame, several analyses of the retrofitted infilled frame were carried out. As a first step, calibration of the tie-model in terms of the effective strain, ε_{te}, the elastic stiffness, K_t, and the post-ultimate softening ratio, p_t, was performed.

Preliminary results (not presented here) showed that, for different reinforcing ratios corresponding to different stories (the 1st story received two TRM layers per side, whereas the 2nd and 3rd stories received one layer per side), the assumption of equal values for the effective strain showed a concentration of damage on the 2nd story. As the latter is not in agreement with the tests, in which the damage was concentrated on the 1st story, the hypothesis that the effective strain decreases with increasing number of externally bonded layers [a well known hypothesis in the case of FRP-strengthened RC members in shear (e.g. Triantafillou and Antonopoulos 2000)], was adopted. In particular, it was assumed that the effective strain is inversely proportional to the square root of $E_t\rho_t$, where E_t is the elastic modulus and ρ_t is the reinforcing ratio of the TRM. Given that E_t is independent of the reinforcing ratio (an assumption not far from reality, as evidenced by the test results on TRM coupons), the effective strain of two layers ($\varepsilon_{te,2layers}$) is 0.707 times that of one layer ($\varepsilon_{te,1layer}$); this value was used in all analyses regarding the retrofitted infilled frame. On the contrary, equal values for the effective strain were used for the two directions of the textile rovings within the same story. As shown in Fig. 14a, the best agreement between the experimental and the numerical analysis results in terms of maximum base shear, was achieved using ε_{te}=0.8% for one TRM layer. Note that a variation in this value of ε_{te} by ±25% resulted in only ±7% variation of the maximum base shear, leading to the conclusion that the global behavior of the infilled frame is non-proportionally sensitive to the value of ε_{te}.

Another parameter under investigation was the effect of the tie elastic stiffness K_t on the global response of the infilled frame. With K_t being inversely proportional to the effective

length of the tie, $L_{e,tie}$ [Eq. (14)], three different values of $L_{e,tie}$ were considered: two extreme values ($0.11L_{tie}$ and $0.5L_{tie}$) and an intermediate one ($0.25L_{tie}$). Again, $L_{e,tie}$ reflects the cracking dispersion length along the tie-diagonal. The first (lower) limit value is the projection of the strut width to the tie-diagonal:

$$L_{e,tie} = \frac{w_{\inf}}{\cos(90^o - 2\theta_{tie})} \tag{15}$$

The second (higher) limit value was set equal to half-length of the tie, provided that all fibers along the considered crack contribute to the tensile force, although they do not have the same length in the tie-diagonal direction. At the point where the crack intersects with the tie-diagonal, this length is equal to the tie-length, whereas at the ends of the crack this length is minimum and equal to zero (when assuming that the crack forms along the strut-diagonal). Finally, the analytical results show that the effect of $L_{e,tie}$, and thus that of K_t, on the global response of the retrofitted infilled frame is negligible and limited only to the global lateral stiffness after diagonal cracking occurs and before the ultimate lateral capacity is reached. As shown in Fig. 14b, use of the intermediate value of $L_{e,tie}$=$0.25L_{tie}$ resulted in the best agreement between the experiment and the analysis, and consequently this value was used for the rest of the analyses.

Figure 14c presents the base shear – top floor displacement envelope curves as obtained from the analyses for three different values of p_t, compared with the experimental response curves. The rather non-symmetric behavior of the post-peak slope of test specimen is attributed to the rupture of fibers at the top boundary of west column-infill on the back side of the 1st story, as explained in Koutas et al. (2014b). The analysis failed to reproduce this type of local damage due to the nature of the model used in this study. Consequently, focusing on the overall response, it is concluded that a value of p_t=0 resulted in the best fit of the analysis to the experiment. Such decision not only simplifies the analytical procedure in terms of the

parameters to be accounted for, but also eliminates the effect of the selected value for $L_{e,tie}$ on the post-ultimate stiffness of the tie (expressed as a fraction of K_{tie}).

The second step taken was to investigate how different sets of values of parameters α and γ affect the analytical results. A series of analyses, with $0 \leq \alpha_t \leq 0.5$ *and* $0 \leq \gamma_t \leq 0.8$, were carried out, with the other parameters taken equal to: $\varepsilon_{te} = 0.8\%$, $L_{e,tie} = 0.5L_{tie}$ and $p_t = 0$. For the whole range of values considered for α_t *and* γ_t the agreement between experimental and numerical results, in terms of both hysteretic energy dissipation and global lateral stiffness, was satisfactory. Figure 15 displays the base shear versus top floor displacement hysteretic curves for three different sets of α_t and γ_t values: (a) $\alpha_t = 0$ and $\gamma_t = 0$, (b) $\alpha_t = 0.4$ and $\gamma_t = 0.4$ and (c) $\alpha_t = 0.5$ and $\gamma_t = 0.8$. The shape of the loops is shown to be only slightly affected, even when comparing the two extreme pairs of α and γ values. Nevertheless, the best agreement between experimental and analytical results is achieved for $\alpha_t = 0.4$ and $\gamma_t = 0.4$ (Fig. 15b). The excellent agreement for this pair of values is also verified in Fig. 16 [in terms of: global stiffness (Fig. 16a), cumulative hysteretic energy (Fig. 16b), and 1st floor displacement prediction (Fig. 16c)], and Fig. 17 (in terms of story shear – interstory drift ratio, for all three stories).

In conclusion, the tie-model developed is proved to simulate with sufficient accuracy the contribution of TRM-retrofitting to the lateral response of the retrofitted infilled frame. The model shows a rather low sensitivity to constituent parameters, except for the effective strain, ε_{te}. Due to lack of experimental data on TRM-strengthened masonry infilled RC frames, this value cannot yet be accurately estimated. Nevertheless, the main objective of this study was to develop a simple integrated analytical procedure comprising both analytical and numerical modeling, in order to serve as a useful tool for future studies in this field.

Conclusions

An analytical procedure for modeling the in-plane behavior of masonry-infilled RC frames strengthened with textile-reinforced mortar (TRM) is presented, based on the use of single-strut and single-tie elements. The values of some of the main parameters of the proposed models for the strut and the tie were obtained from experimental results on sub-assemblies, which are also presented in this study. Finally, several numerical analyses were carried out after implementing the modeling scheme into the open-source software *OpenSees* and the results were compared with experimental data obtained from cyclic tests on two three-story masonry infilled RC frames.

A general conclusion is that the proposed modeling scheme can adequately reproduce the experimental response of both the un-retrofitted and the retrofitted infilled frame. The model for the strut employed was validated by comparison with experimental results of the un-retrofitted infilled frame, while experimental results of the retrofitted infilled frame were used for calibrating the model for the tie. The behavior of the tie under tension was idealized as bilinear with simple hysteresis rules similar to those used for the model of the strut. The key parameter of the tie-model is the effective strain. In view of the lack of sufficient data, the best agreement between the experiment and the analysis was achieved for a value of the effective strain equal to 0.8%, when one layer of TRM is employed. The model developed for the tie is flexible and shown not to be appreciably sensitive to other parameters.

This study is the first attempt to model masonry infilled RC frames strengthened with TRM and focuses mainly on the contribution the TRM layers offer to the global response. Future research could provide more experimental data for both the calibration of the value of the effective strain and the comparison – and eventual adjustment – of the current model with test results from TRM-retrofitted, masonry-infilled structures other than those on which it was based.

Acknowledgements

This research has been co-financed by the European Union (European Social Fund – ESF) and Greek national funds through the Operational Program "Education and Lifelong Learning" of the National Strategic Reference Framework (NSRF) - Research Funding Program HERACLEITUS II - Investing in knowledge society through the European Social Fund. The authors wish to thank Assoc. Prof. Christis Chrysostomou for his input on modeling aspects, the graduate student Stavroula Skafida for her advice on the numerical simulations and the undergraduate students A. Mystiliadi, E. Argyropoulou and K. Kefalou for their assistance in different parts of the experimental program.

References

Akin, E., Özcebe, G., Canbay, E., and Binici, B. (2014). "Numerical study on CFRP strengthening of reinforced concrete frames with masonry infill walls." *J. Compos. Constr.*, 18(2), 04013034, doi: 10.1061/(ASCE)CC.1943-5614.0000426.

Al-Salloum, Y. A., Siddiqui, N. A., Elsanadedy, H. M., Abadel, A. A., and Aqel, M. A. (2011). "Textile-reinforced mortar versus FRP as strengthening material for seismically deficient RC beam-column joints." *J. Compos. Constr.*, 15(6), 920-933.

Asteris, P. G., Antoniou, S. T., Sophianopoulos, D. S., and Chrysostomou, C. Z. (2011). "Mathematical macro-modeling of infilled frames: state-of-the art." *J. Struct. Eng.*, 137(12), 1508–1517.

ASTM E519-10 (2010). "Standard test method for diagonal tension (shear) in masonry assemblages." West Conshohocken, PA.

Babaeidarabad, S., De Caso, F., and Nanni, A. (2014). "URM walls Strengthened with fabric-reinforced cementitious matrix composite subjected to diagonal compression." *J. Compos. Constr.*, 18(2), 04013045, doi: 10.1061/(ASCE)CC.1943-5614.0000441.

Binici, B., and Ozcebe, G. (2006). Analysis of infilled reinforced concrete frames strengthened with FRPs." Wasti, S. T, and Ozcebe, G. (eds). Advances in earthquake engineering for urban risk reduction. NATO Science Series, Earth and Environmental Sciences, vol. 66. Springer, p. 455–71.

Bournas, D. A., Lontou, P., Papanicolaou, C. G., and Triantafillou, T. C. (2007). "Textile-reinforced mortar (TRM) versus FRP confinement in reinforced concrete columns." *ACI Struct. J.*, 104(6), 740-748.

Bournas, D. A., Triantafillou, T. C., Zygouris, K., and Stavropoulos, F. (2009). "Textile-reinforced mortar versus FRP jacketing in seismic retrofitting of RC columns with continuous or lap-spliced deformed bars." *J. Compos. Constr.*, 13(5), 360–371.

Chrysostomou, C. Z., and Asteris, P. G. (2012). "On the in-plane properties and capacities of infilled frames", *Eng. Struct.*, 41, 385-402.

D'Ambrisi, A., and Focacci, F. (2011). "Flexural strengthening of RC beams with cement-based composites." *J. Compos. Constr.*, 15(5), 707-720.

Dizhur, D., Griffith, M., and Ingham, J. (2013). "In-plane shear improvement of unreinforced masonry wall panels using NSM CFRP strips." *J. Compos. Constr.*, 17(6), 04013010, doi: 10.1061/(ASCE)CC.1943-5614.0000400.

Dolsek, M., and Fajfar, P. (2002). "Mathematical modeling of an infilled RC frame structure based on the results of peudo-dynamic tests." *Earthquake Engng. Struct. Dyn.,* 31, 1215-1230.

EN 1015-11 (1993). "Methods of test for mortar for masonry – Part 11: Determination of flexural and compressive strength of hardened mortar." Comité Européen de Normalisation, Brussels.

EN 1052-1 (1999). "Methods of test for masonry – Part 1: Determination of compressive strength." Comité Européen de Normalisation, Brussels.

EN 1998–3 (2005). "Eurocode 8: design of structures for earthquake resistance – part 3: assessment and retrofitting of buildings." Comité Européen de Normalisation, Brussels.

Erol, H. F., Karadogan, H. F., and Cili, F. (2012). "Seismic strengthening of infilled reinforced concrete frames by CFRP." *Proc. 15 WCEE*, Lisboa, Portugal.

Fardis, M. N., and Panagiotakos, T. B. (1997). "Seismic design and response of bare and masonry-infilled reinforced concrete buildings Part II: infilled structures." *J. Earthquake Eng.*, 1(3), 475-503.

Fardis, M. N. (2009) "Seismic design, assessment and retrofitting of concrete buildings: based on EN-Eurocode 8." 1st ed., Springer, Netherlands.

Harajli, M., ElKhatib, H., and Tomas San-Jose, J. (2010). "Static and cyclic out-of-plane response of masonry walls strengthened using textile-mortar system." *J. Mater. Civ. Eng.*, 22(11), 1171-1180.

Ibarra, L. F., and Krawinkler, H. (2005). "Global collapse of frame structures under seismic excitations." Rep. No. TB 152, The John A. Blume Earthquake Engineering Center, Stanford University, Stanford, CA.

Kappos, A. J., Stylianidis, K. C., and Michailidis, C. N. (1998). "Analytical models for brick masonry infilled R/C frames under lateral loading." *J. Earthquake Eng.*, 2(1), 59-87.

Koutas, L., Pitytzogia, A., Triantafillou, T. C., and Bousias, S. N. (2014a). "Strengthening of infilled reinforced concrete frames with TRM: Study on the development and testing of textile-based anchors." *J. Compos. Constr.*, 18(3), A4013015, doi:10.1061/(ASCE)CC.1943-5614.0000390.

Koutas, L., Bousias. S.N., and Triantafillou, T. C. (2014b). "Seismic strengthening of masonry-infilled RC frames with TRM: Experimental study." *J Compos Constr,* , 04014048, doi: 10.1061/(ASCE)CC.1943-5614.0000507.

Koutromanos, I., Stavridis, A., Shing, P. B., and Willam, K. J. (2011). "Numerical modeling of masonry-infilled RC frames subjected to seismic loads." *Comput. Struct.*, 89(11–12), 1026–1037.

Koutromanos, I., and Shing, P. B. (2014). "Numerical study of masonry-infilled RC frames retrofitted with ECC overlays." *J. Struct. Eng.*, 140(7), 04014045, doi: 10.1061/(ASCE)ST.1943-541X.0000934.

Krevaikas, T. D., and Triantafillou, T. C. (2005). "Computer-aided strengthening of masonry walls using fibre-reinforced polymer strips", *Mater. Struct.,* 38, 93-98.

Madan, A, Reinhorn, A. M., Mander, J. B., and Valles, R.E. (1997). "Modeling of masonry infill panels for structural analysis." *J. Struct. Eng.*, 123(10), 1295-1302.

Mainstone, R. J. (1971). "On the stiffnesses and strengths of infilled frames." *Proc. Inst. Civil Eng.*, Suppl. Iv, 57–90, (7360 S).

McKenna, F., Fenves, G. L., Scott, M. H., and Jeremic, B. (2000). "Open System for Earthquake Engineering Simulation (OpenSees)." Pacific Earthquake Engineering Research Center, University of California, Berkeley, CA.

Papanicolaou, C. G., Triantafillou, T. C., Karlos, K., and Papathanasiou, M. (2007). "Textile-reinforced mortar (TRM) versus FRP as strengthening material of URM walls: in-plane cyclic loading." *Mater. Struct.*, 40(10), 1081-1097.

Papanicolaou, C. G., Triantafillou, T. C., Papathanasiou, M., and Karlos, K. (2008). "Textile-reinforced mortar (TRM) versus FRP as strengthening material of URM walls: out-of-plane cyclic loading." *Mater. Struct.*, 41(1), 143-157.

Parisi, F., Iovinella, A., Balsamo, A., Augenti, N., and Prota, A. (2013). "In-plane behavior of tuff masonry strengthened with inorganic matrix–grid composites." *Compos: Part B*, 45(1), 1657-1666.

Paulay, T., and Priestley, M. J. N. (1992). "Seismic design of reinforced concrete and masonry buildings." John Wiley & Sons, New York.

RILEM TC 76-LUM (1994). "Diagonal tensile strength tests of small wall specimens." Bagneux: International Union of Laboratories and Experts in Construction Materials, Systems and Structures.

Saneinejad, A., and Hobbs, B. (1995). "Inelastic design of infilled frames." *J. Struct. Eng.*, 121(4), 634–650.

Skafida, S., Koutas, L., and Bousias, S. N. (2014). "Analytical modeling of masonry infilled RC frames and verification with experimental data." *J. Struct. (Hindawi),* Article ID 216549, 17 pages, doi:10.1155/2014/216549.

Stafford Smith, B., and Carter, C. (1969). "A method of analysis for infilled frames." *Proc. Inst. Civil. Eng.*, 44(1), 31–48, London.

Stylianidis, K. C. (1985). "Experimental investigation of the behaviour of the single-story infilled RC frames under cyclic quasi-static horizontal loading (parametric analysis)." Ph.D. Thesis, Department of Civil Engineering, Aristotle University of Thessaloniki, Thessaloniki, Greece.

Takeda, T., Sozen, M.A., and Nielsen, N. N. (1970). "Reinforced concrete response to simulated earthquakes." *J. Struct. Div*., 96(ST12), 2257-2573.

Triantafillou, T. C., and Antonopoulos C. P. (2000). "Design of concrete flexural members strengthened in shear with FRP." *J. Compos. Constr.,* 4(4), 198–205.

Triantafillou, T. C., and Papanicolaou, C. G. (2006). "Shear strengthening of RC members with textile reinforced mortar (TRM) jackets." *Mater. Struct.*, 39(1), 85-93.

Triantafillou, T. C., Papanicolaou, C. G., Zisimopoulos, P., and Laourdekis, T. (2006). "Concrete confinement with textile reinforced mortar (TRM) jackets." *ACI Struct. J.*, 103(1), 28-37.

Zarnic, R., Tomazevic, M. (1985). "Study of the behaviour of masonry infilled reinforced concrete frames subjected to seismic loading – Part II." *Rep. ZRMK/lKPl-85/02*, Ljubljana, Slovenia.

List of Figures

parameter values α=0.15, β=0.1 and γ=0.8; and (c) base shear versus top floor displacement curves for strut model parameter values α=0.15, β=0.2 and γ=0.3.

Fig. 13 Comparison between analysis and experimental results for the unretrofitted infilled frame, for α=0.15, β=0.2 and γ=0.3, in terms of: (a) global lateral stiffness per cycle; (b) cumulative global hysteretic energy; and (c) peak positive and negative first floor displacements per cycle.

Fig. 14 Comparison between analysis and experimental results for the retrofitted infilled frame; calibration of the tie model in terms of: (a) the effective strain, ε_{te}; (b) the effective length, $L_{e,tie}$; and (c) the post-ultimate stiffness softening ratio, p_t.

Fig. 15 Comparison between analysis and experimental results for the retrofitted infilled frame; base shear versus top floor displacement hysteretic curves for three different sets of α_t and γ_t values: (a) α_t=0 and γ_t=0; (b) α_t=0.4 and γ_t=0.4; and (c) α_t=0.5 and γ_t=0.8.

Fig. 16 Comparison between analysis and experimental results for the retrofitted infilled frame, for α_t=0.4, β_t=0 and γ_t=0.4, in terms of: (a) global lateral stiffness per cycle; (b) cumulative global hysteretic energy; and (c) peak positive and negative first floor displacements per cycle.

Fig. 17 Comparison between analysis and experimental results for the retrofitted infilled frame; story shear force versus interstory drift ratio hysteretic curves for each story.

Table 1. Properties of the textile.

Property	Polymer coated E-glass fibers textile; Property value
Mesh size	25x25 mm
Weight	405 g/m^2
Weight distribution in the two main directions	50-50 %
Tensile strength per running meter	115 kN/m[a]
Rupture strain	2.5 % [a]
Modulus of elasticity	73 GPa
Fiber density	2.6 g/cm^3

[a] Taken from data sheets of the manufacturer.

Table 2. TRM coupons tensile tests results.

Group	No. of layers	Direction angle α	Maximum stress f_t [a]		Strain at ultimate load ε_{tu}		Elastic modulus E_t [b]	
			Mean value (MPa)	CoV (%)	Mean value (%)	CoV (%)	Mean value (GPa)	CoV (%)
1A	1	0^o	11.9	3.2	1.94	10.8	0.62	11.3
1B	1	90^o	11.3	6.3	1.51	6.6	0.75	2.7
2A	2	0^o	9.5	11.6	1.90	27.1	0.52	17.3
2B	2	90^o	9.6	5.2	1.29	7.7	0.75	6.7

[a] Nominal stress calculated on the basis of the nominal thickness of TRM (4 mm per textile layer).
[b] Secant modulus of elasticity obtained from 0 to 100% of the nominal stress-strain curve.

Table 3. Results of compression tests on masonry wallettes.

Group	No. of TRM layers	Compressive strength f_m [a]		Secant elastic modulus E_m [b]	
		Mean value (MPa)	CoV (%)	Mean value (GPa)	CoV (%)
Unretrofitted	-	5.1	12.8	3.37	2.1
Retrofitted	2	5.7	6.5	3.42	3.5

[a] Stress calculated on the basis of the thickness of the wallette, not including the thickness of any additional layers of TRM.
[b] Secant modulus of elasticity obtained from 5 to 33% of the compressive strength.

Table 4. Results of diagonal compression tests on masonry wallettes.

Group	No. of layers	Diagonal cracking stress τ_{cr} [a]		Shear modulus G	
		Mean value (MPa)	CoV (%)	Mean value (GPa)	CoV (%)
DC_CON	-	0.39	27.8	1.38	26.5
DC_1L	1	0.60	18.9	1.90	20.6
DC_2L	2	0.85	6.8	2.65	10.0

[a] Not accounting for the TRM layers thickness.

Table 5. Properties used to model the plastic hinges of the RC frame members.

Property	Columns			Beams (all stories)	
	1st story	2nd story	3rd story	All stories	
	±	±	±	+	-
Yield Moment, M_y (kNm)	41.5	38.2	34.9	37.8	64.2
Ultimate Moment, M_u (kNm)	41.5	38.2	34.9	37.8	64.2
Chord rotation at yielding, θ_y (rad)	0.0112	0.0109	0.0107	0.0076	0.01
Ultimate chord rotation, θ_{um} (rad)	0.0341	0.0358	0.0375	0.0704	0.0534
Unloading stiffness parameter, *beta* (see McKenna et al. 2000)	0.5	0.5	0.5	0.5	0.5

Table 6. Properties of strut elements as used in the analyses.

Property		Unretrofitted infilled frame (all stories)	Retrofitted infilled frame	
			1st story	2nd, 3rd story
θ_{str}		36°	36°	36°
λH	(m)	3.75	3.75	3.75
t_w	(mm)	110	110	110
w_{inf}	(mm)	289	289	289
τ_{cr}	(MPa)	0.39[a]	0.85[a]	0.60[a]
f_w	(MPa)	5.1[a]	5.7[a]	5.4[b]
E_w	(GPa)	3.37[a]	3.42[a]	3.40[b]
V_{cr}	(kN)	97.5	212	150
G	(GPa)	1.38[a]	2.65[a]	1.90[a]
K	(kN/mm)	209	401	288
V_u	(kN)	225	252	238

[a] Taken from the results of masonry sub-assemblies tests.

[b] Estimated assuming a proportional increase in compressive strength as the number of TRM layers increases.

Table 7. Properties of tie elements used in the analyses.

Property		Retrofitted infilled frame	
		1st story	2nd, 3rd story
α_1		0°	0°
α_2		90°	90°
β_1		54°	54°
β_2		36°	36°
θ_{tie}		36°	36°
θ_1		45°	45°
H_{con}	(mm)	289	289
$L_{cr,1}$	(mm)	1923	1923
$L_{cr,2}$	(mm)	910	910
$E_{t,1}$	(GPa)	0.52[a]	0.6 [a]
$E_{t,2}$	(GPa)	0.75[a]	0.75[a]
$A_{t,1}$	(mm^2)	400[b]	200[c]
$A_{t,2}$	(mm^2)	400[b]	200[c]

[a] Taken from the results of TRM coupons tests.

[b] By using n_s=2, n_t=2, t_t=4mm and $mesh,1 = mesh,2$ = 25 mm in Eq. (12).

[c] By using n_s=2, n_t=1, t_t=4mm and $mesh,1 = mesh,2$ = 25 mm in Eq. (12).

Figures

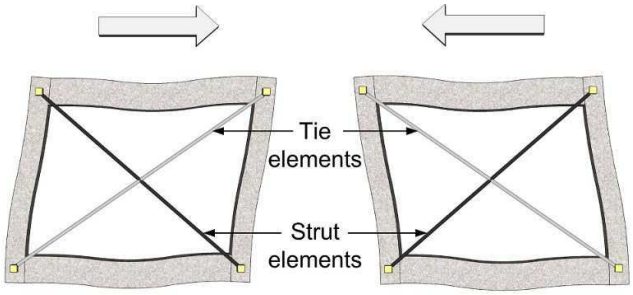

Fig. 1

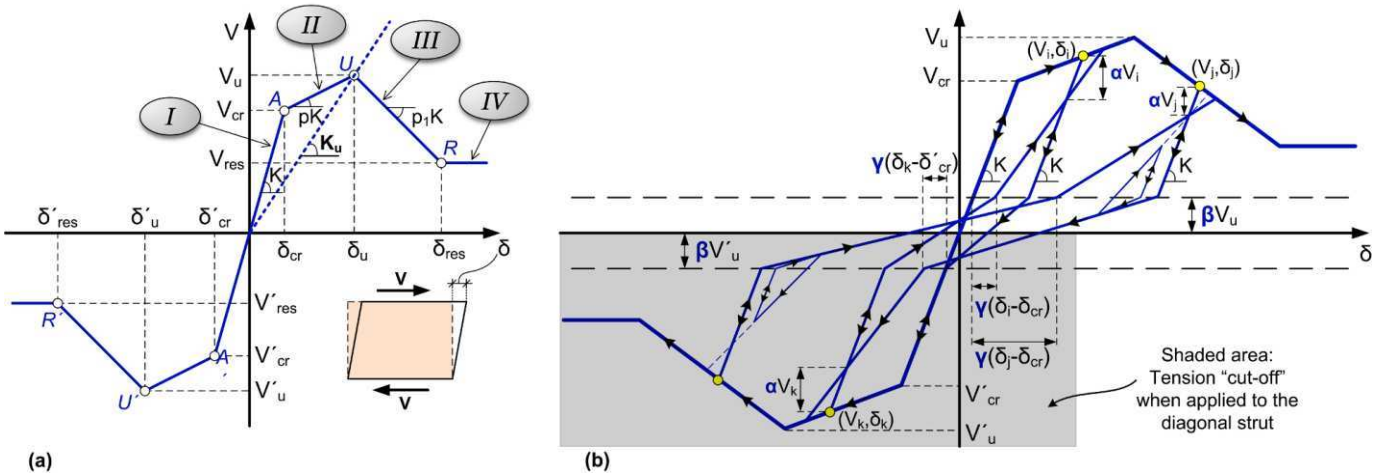

Fig. 2

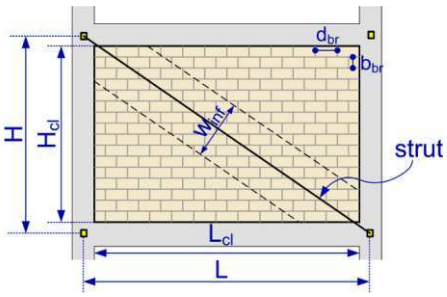

Fig. 3

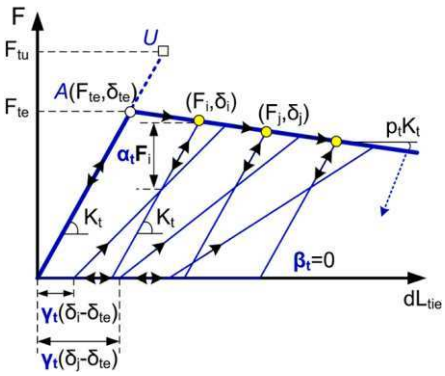

Fig. 4

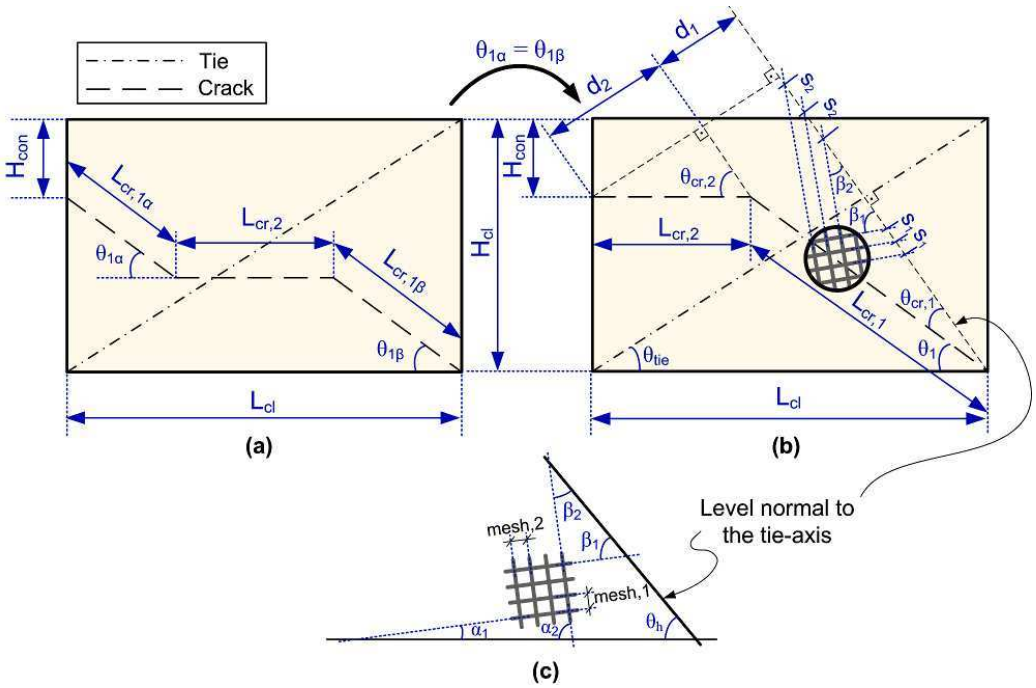

Fig. 5

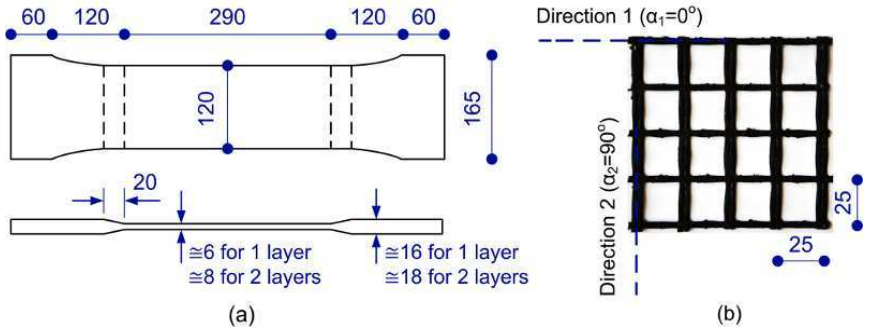

Fig. 6

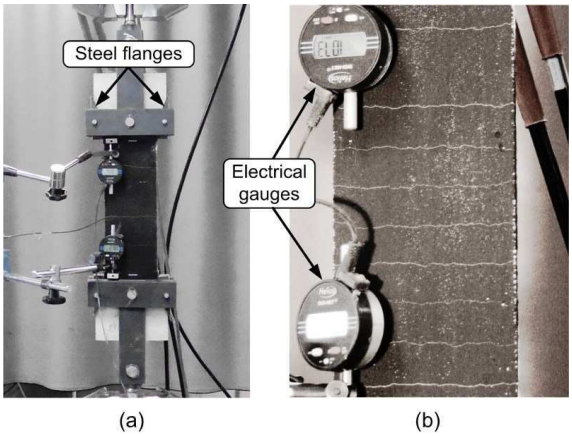

Fig. 7

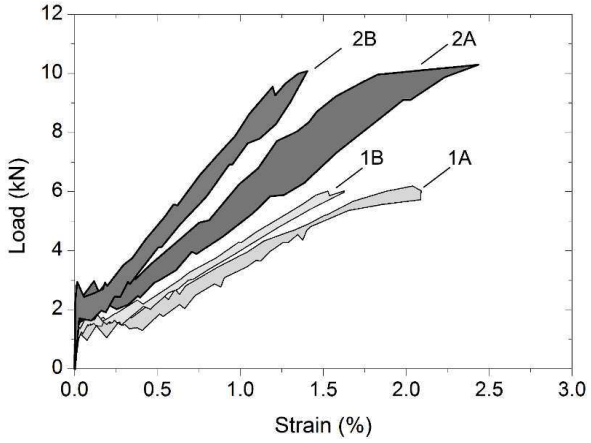

Fig. 8

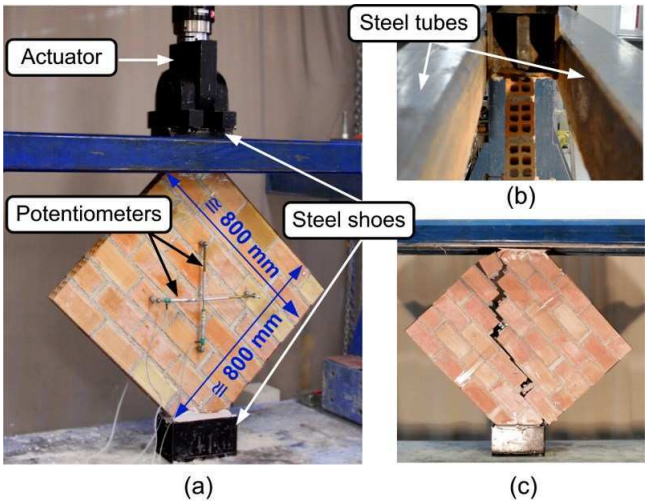

Fig. 9

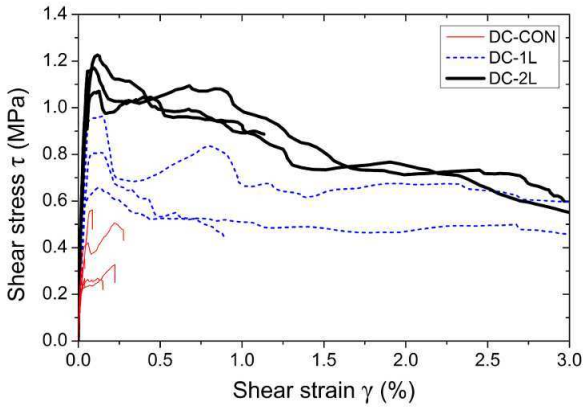

Fig. 10

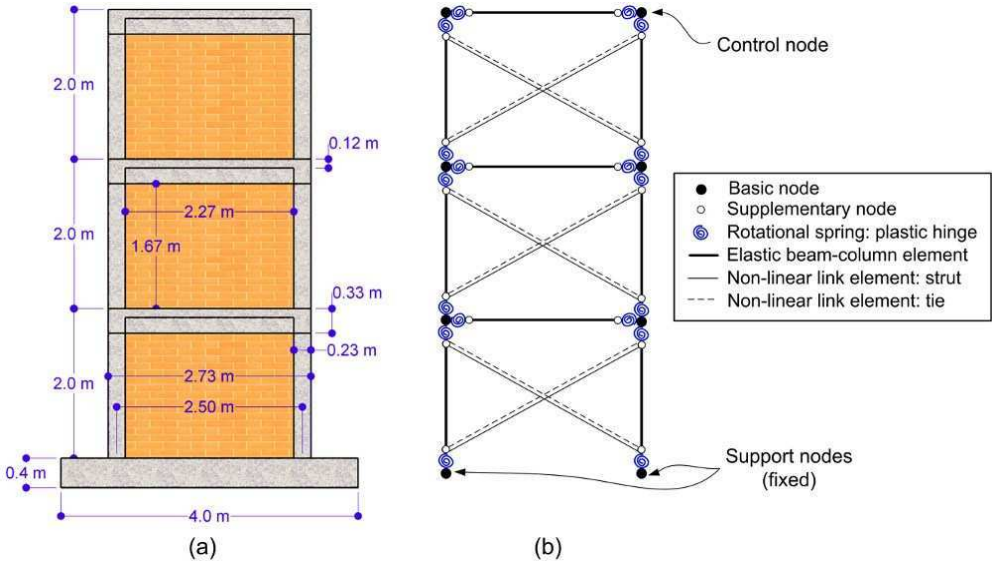

Fig. 11

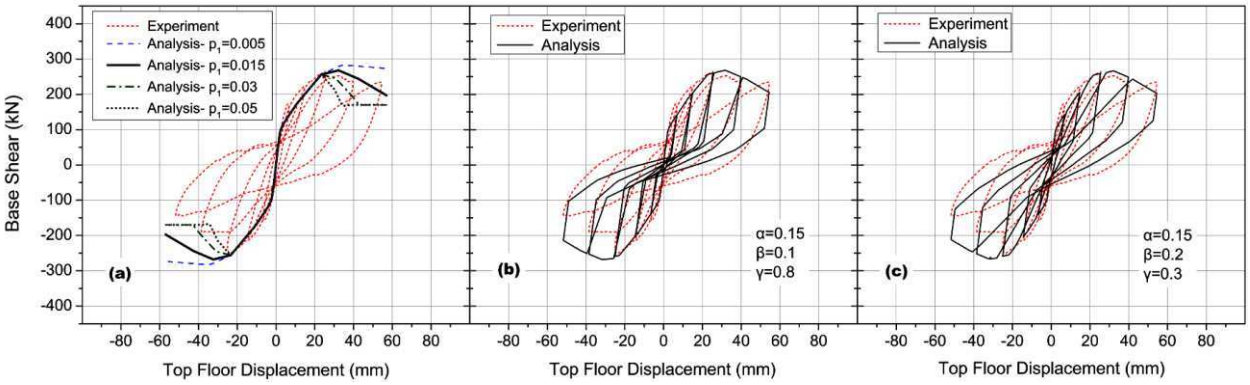

Fig. 12

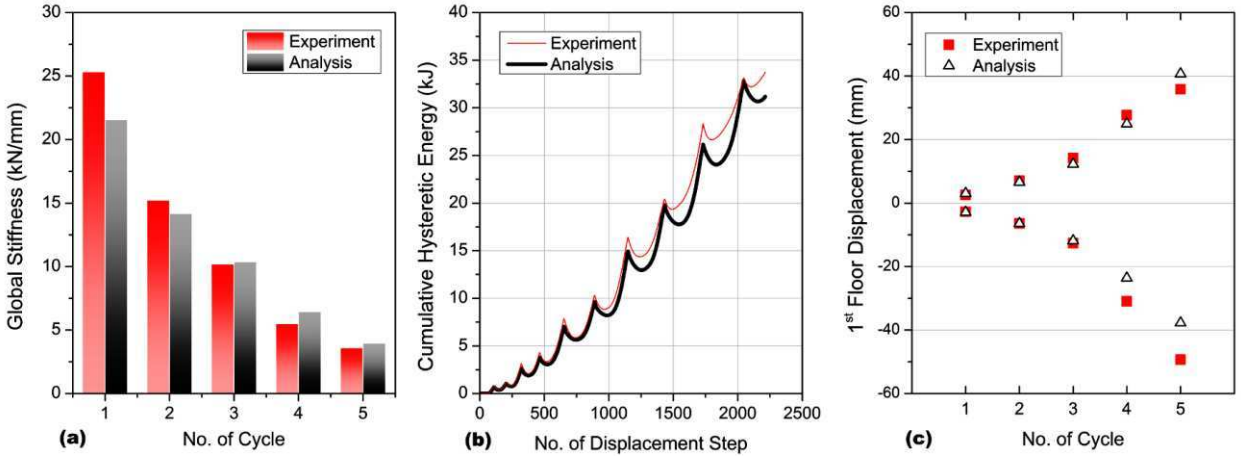

Fig. 13

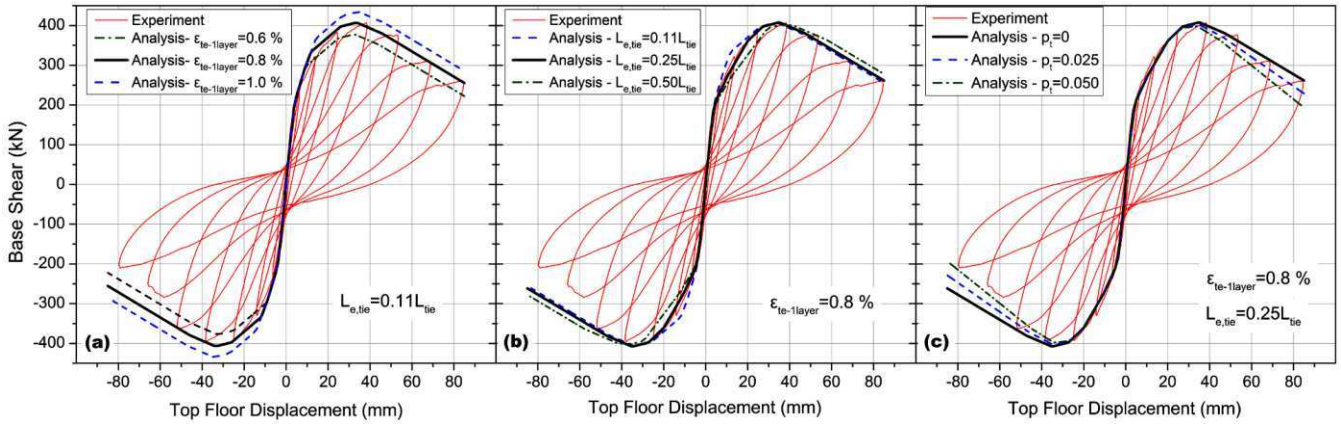

Fig. 14

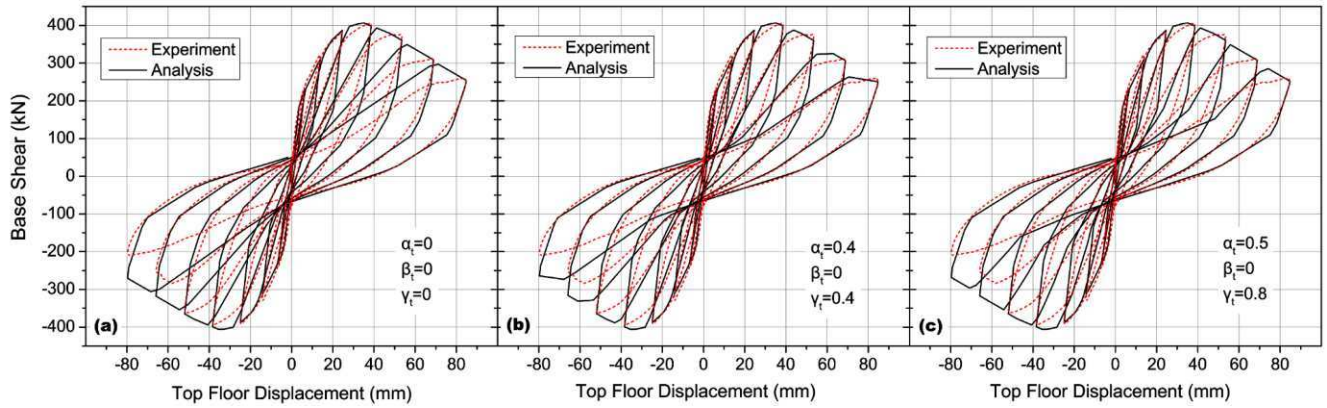

Fig. 15

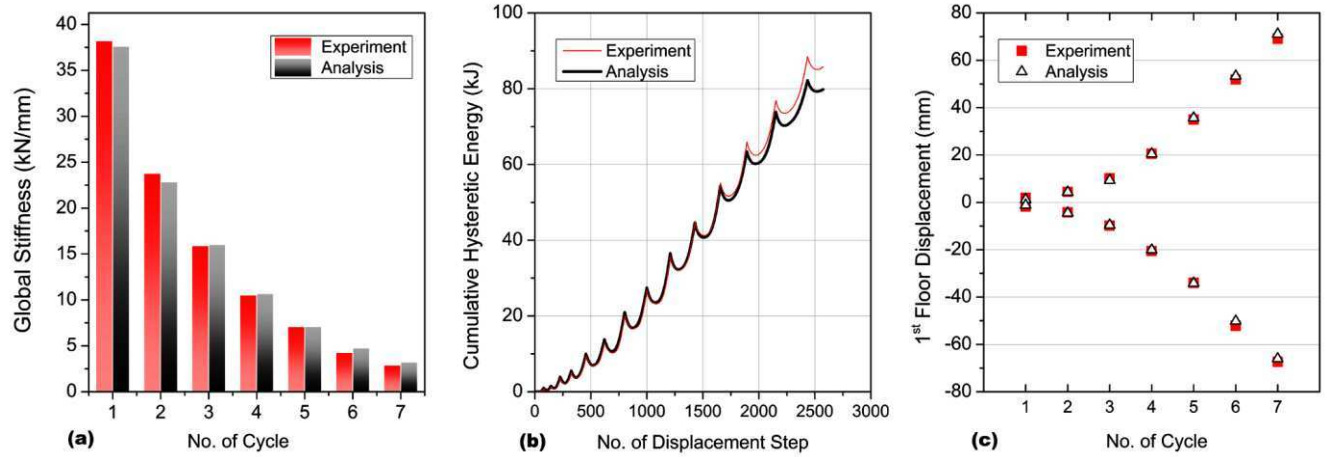

Fig. 16

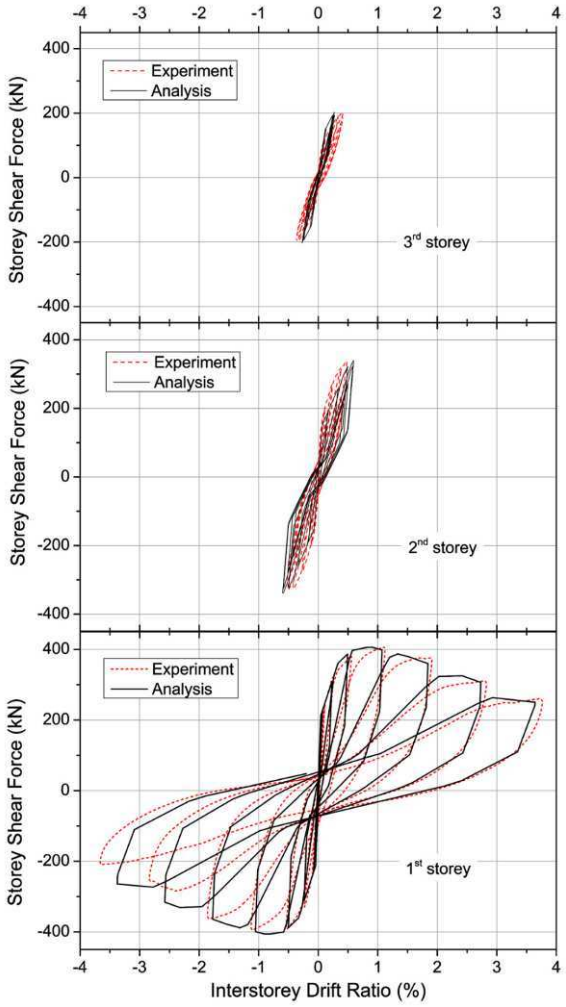
Experiment
Analysis
3rd storey
2nd storey
1st storey
Storey Shear Force (kN)
Interstorey Drift Ratio (%)

Fig. 17